Catena 203 (2021) 105317

Contents lists available at ScienceDirect

Catena

journal homepage: www.elsevier.com/locate/catena

# Slow-moving landslide risk assessment combining Machine Learning and InSAR techniques

A. Novellino [a,*], M. Cesarano [b], P. Cappelletti [b], D. Di Martire [b], M. Di Napoli [c], M. Ramondini [d], A. Sowter [e], D. Calcaterra [b]

[a] British Geological Survey, Environmental Science Centre, Keyworth, Nottingham NG12 5GG, UK
[b] Department of Earth, Environment and Resources Sciences, Federico II University of Naples, Naples 80138, Italy
[c] Department of Earth, Environmental and Life Sciences, University of Genoa, Genoa 16132, Italy
[d] Department of Civil, Architectural and Environmental Engineering, Federico II University of Naples, Naples 80125, Italy
[e] Terra Motion Limited, Ingenuity Centre, Nottingham NG7 2TU, UK

ARTICLE INFO

*Keywords:*
Landslides
InSAR
Machine Learning Algorithms
Landslide hazard
Landslide risk

ABSTRACT

This paper describes a novel methodology where Machine Learning Algorithms (MLAs) have been integrated to assess the landslide risk for slow moving mass movements, processes whose intermittent activity makes challenging any risk analysis worldwide.

MLAs has been trained on datasets including Interferometric Synthetic Aperture Radar (InSAR) and additional remote sensing datasets such as aerial stereo photographs and LiDAR and tested in the Termini-Nerano landslides system (southern Apennines, Italy).

The availability of such a wealth of materials allows also an unprecedented spatio-temporal reconstruction of the volume and the kinematic of the landslides system through which we could generate and validate the hazard map.

Our analysis identifies fifteen slow-moving phenomena, traceable since 1955, whose total area amounts to 4.1 $\times 10^5$ m$^2$ and volume to ~1.4 $\times 10^6$ m$^3$. InSAR results prove that seven out of the fifteen slow-moving landslides are currently active and characterized by seasonal velocity patterns. These new insights on the dynamic of the landslides system have been selected as the main independent variables to train three MLAs (Artificial Neural Network, Generalized Boosting Model and Maximum Entropy) and derive the landslide hazard for the area. Finally, official population and buildings census data have been used to assess the landslide risk whose highest values are located in the crown area, south of Termini village, and nearby Nerano.

This new methodology provides a different landslide risk scenario compared to the existing official documents for the study area and overall new insights on how to develop landslide risk management strategies worldwide based on a better understanding of slope processes thanks to the latest satellite technologies available.

## 1. Introduction

Landslides are ubiquitous in any terrestrial environment with slopes, driven by tectonic, climatic and/or human activities (Froude and Petley, 2018). In particular, slow-moving landslides, which move downslope for months to decades at rates ranging from millimetres to several metres per year, provide an excellent opportunity to study landslide processes (Lacroix et al., 2020). Even if slow-moving landslides rarely claim lives, they still cause widespread destruction and if they rapidly accelerate result in casualties (Handwerger et al., 2019).

Slow-moving landslide events are recurring phenomena in southern Italy (e.g., Novellino et al., 2015; Di Martire et al., 2016; Pappalardo et al., 2018) due to its geological history and tectonic-geomorphological evolution which resulted in the occurrence of several formations identified as Structurally Complex Formations (SCFs; Esu, 1977), flysches or Broken Formations (Mutti et al., 2009). The term refers to geological units constituted by lithologically mixed terrains with extra-formational blocks (D'Elia et al., 1998), associable to the preorogenic and synorogenic turbidites of the Alps-Apennine system (Alvarez, 1991). Such tectonic activity also contributed to the poor mechanical properties of

* Corresponding author.
*E-mail address:* alessn@bgs.ac.uk (A. Novellino).

https://doi.org/10.1016/j.catena.2021.105317
Received 8 September 2020; Received in revised form 2 February 2021; Accepted 13 March 2021

the SCFs that represent one of the main factors contributing to the predisposition of slopes to landslide (Del Soldato et al., 2018). The latest Inventory of Landslide Phenomena in Italy report (IFFI) carried out by the Italian National Institute for Environmental Protection and Research (ISPRA, 2018) evidences that slides, flows and composite phenomena (Hungr et al., 2014)). account for ~30% of the 620,808 mass movements inventoried in Italy. These three types of movements are typical of instabilities generated in SCFs (Fig. 1a), which have a huge impact on the Italian socio-economic system (Salvati et al., 2010) due to the shorter return periods (Fig. 1b) and higher spatial density (Fig. 1c) than landslides generated in other types of terrains.

The variability of material properties and landslide kinematics in SCFs, with a long state of activity at intermittent rates of displacement, makes any estimation of the corresponding risk challenging. To this respect, field-based monitoring systems (e.g., extensometers, crack meters, inclinometers, GNSS receivers) only provides spatially discontinuous, costly, labour intensive and time-consuming information. On the contrary, the use of remote sensing methods, like Interferometric Synthetic Aperture Radar (InSAR) represents a time-saving and cost-effective approach for understanding landslides kinematics (Novellino et al., 2017), namely the hazard and deriving the corresponding risk. Landslide hazard is the likelihood of a potentially damaging landslide occurring within a given area with landslide risk being the spatio-temporal probability of the expected losses to life and damage to property, should a landslide occur (van Westen et al., 2008) and landslide risk maps (LRMs) represent essential tools for effective land use management and planning (Fell et al., 2008). Given the high number of events, the challenge of assessing landslide risk related to slow-moving phenomena is particularly evident in Italy where this mandate, since 1998, belongs to the River Basin Authorities (recently merged in eight national Hydrographic Districts). River Basin Authorities have produced landslide hazards and risk maps which cover the whole Italian territory at scale ranging between 1:5,000 to 1:25,000. These maps represent official tools for land use and urban planning activities but are limited by common drawbacks: are usually produced from input datasets not regularly updated and mainly based on data-driven empirical methods which do not account for characteristics such as landslide velocity or the uncertainty in the maps themselves.

Despite various recent initiatives (Confuorto et al., 2017; Hu et al., 2020), the use of multidisciplinary approaches where InSAR has been deployed for a complete analysis of landslide kinematics and driving mechanisms is still limited and, consequently, the translation of these information in LRMs is even rarer so resulting in the absence of measures sufficient for landslide risk management/reduction.

The aim of this study is therefore to develop and validate a new methodology to assess landslide risk for slow-moving landslides based on Machine Learning Algorithms (MLAs). Recently, MLAs and in particular Ensemble Modelling (EM) has provided a solid contribution to minimize the uncertainty and improve the reliability of landslide mapping prediction by accounting for different data-driven methods together (Chen et al., 2017). To this, Ensemble methods have been proposed to combine the advantages of each stand-alone models and to mitigate the effects of their drawbacks (Thuiller et al., 2009).

In this work, we have trained three MLAs, Artificial Neural Network (ANN), Generalized Boosting Model (GBM) and Maximum Entropy (MaxEnt) with geological, geomorphometric and, for the first time, InSAR datasets to obtain a relative landslide hazard map. The latter has been then combined with data from the population and building environment to derive a relative risk map. MLAs methodologies have been recently applied in the literature to rapid landslides (Di Napoli et al., 2020) but, to our knowledge, not yet to slow ones.

MLAs have proven to outperform, especially at catchment and regional scale, heuristic and statistical models as they can address the nonlinear corrections between landslides and conditioning factors and can determine model parameters automatically (Huang et al., 2020). We tested our method for an area which has experienced rapid urban expansion first and tourism then: Termini-Nerano (southern Italy). Specifically to the area of study, our work has allowed to update the existing inventory map dated 2011 and compiled by the Southern Apennines Hydrographic District (SAHD, 2011a) and then improve the existing landslide risk map (SAHD, 2011b). More generally, our new methodology has already potential to be implemented at national and continental scale and, provided that the input data are available, easily applied worldwide.

The paper is organized as follows: a description of the geological-geomorphological setting of the Termini-Nerano site with a brief description of the landslide event history is provided in Section 2; the methodological approach developed for assessing the landslide risk is described in Section 3 along with the datasets used. The results are shown in Section 4 followed by the discussion and conclusions in Section 5 and 6, respectively, where we analyse why and how our approach can be extended elsewhere.

## 2. The Termini-Nerano landslides system

The studied area is located on the south-facing coast of the Sorrento

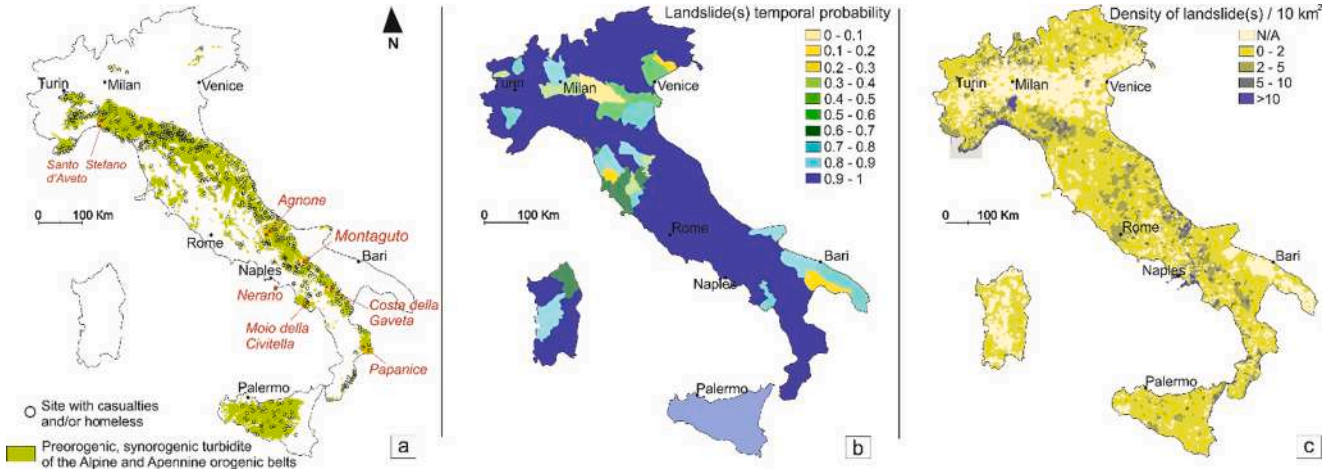


**Fig. 1.** Spatial distribution of landslides resulting in casualties and/or homeless in Italy between 650 and 2008 (modified from Salvati et al., 2010) within SCFs-like outcropping units mapped following the 1:250,000 geological map of Italy (available at: http://www.isprambiente.gov.it/en/projects/soil-and-territory/the-geological-map-of-italy-1-250000-scale/default) with location of well-known landslides in SCFs from the literature (a). Landslide temporal probability between 2018 and 2028 in Italy (b). Landslide density in Italy (c). Landslide data are available at: http://webmap.irpi.cnr.it/webmap_test/webmap.html.

Peninsula, southern Italy (Fig. 2) where the landslide system affects three villages, Termini, Nerano and Marina del Cantone. Geologically, the Termini-Nerano area belongs to the shallow-water carbonates succession of the Lattari-Picentini Unit, in the western sector of the Apennine Carbonate Platform (Vinci et al., 2017). According to ISPRA (2015), the outcropping rocks are composed of pre-orogenic Mesozoic carbonate sequence of the Radiolitidae limestone Formation (Upper Cretaceous; Iannace et al., 2011) topped by synorogenic terrigenous deposits of Miocene age including the Recommone Calcarenites Formation (Lower Miocene), the Termini Sandstones Formation (TSF - Miocene) and the Punta del Capo Breccias (Upper Miocene; D'Argenio et al., 2011). Quaternary deposits consist of slope debris, derived from the limestone and sandstone bedrock, pyroclastic, and beach deposits. The latter cover the bedrock succession at limited spots, such as Marina del Cantone, but not at the Termini-Nerano valley. The Miocene TSF (200 m thick) is divided into two members: the lowermost is the Nerano Member where the studied landslides developed. It consists of arkosic sandstones, interbedded with siltstone and mudstone levels, cropping out south of Termini. A gradual vertical and lateral transition leads to the Marciano Member, a thin-bedded arkosic turbiditic sandstone succession interbedded with marly levels. The tectonic features which most influence the local geomorphology are connected to a first compressional event with a NE-vergence, followed by an extensional one (ISPRA, 2015). The compressive phase created gentle folds in the TSF with the Upper Cretaceous carbonates thrusting over the TSF (Vitale et al., 2017) and determined the attitude of the Nerano Member to be converging towards the valley centre (Fig. 2).

The mesoscopic scaly texture of the clayey intervals combined with the strong tectonic deformation and the presence of calcareous exotic blocks in the TSF, represent an important predisposing factor to slope instability in the area and a classical example of a SCF with geotechnical properties intermediate between soils and rocks, strongly dependent on the scale of the mechanical discontinuities.

According to historical chronicles, archive documents, local witnesses and data from the Italian National Research Council (Canuti et al., 1992; de Riso et al., 2004), the valley has been affected by several instability events in the recent past. The oldest phenomenon reported occurred in the 17th century with successive reactivations recorded in 1910, 1939, in late December 1940 and early January 1941. The latter involved a $2.1 \times 10^5$ m$^2$ area and a $2 \times 10^6$ m$^3$ volume and destroyed the Termini-Capo d'Arco road and some houses in Termini (Brugner and Valdinucci, 1973). The following reactivation took place in Capo D'Arco hill, northeast of the village of Termini, on 19th of February 1963 and lasted seven days (Cotecchia and Melidoro, 1966). The event was triggered after 101 mm of cumulative rainfall in the previous 24 h and 217.4 mm in the previous 19 days, corresponding to almost 20% of the 1963 annual rainfall budget. Landslide velocity ranged from 3 m/h to 27 m/h (Cotecchia and Melidoro, 1966); the movement started as a rotational slide and then developed as a flow that struck the villages of Nerano and Marina del Cantone, ~900 m downslope, before reaching the Tyrrhenian Sea. Seismic refraction studies in the aftermath of the event localized the main rupture surface at ~25 m of depth (Cotecchia and Melidoro, 1966) and reported a total length of the landslide body of ~1,900 m with an area of $1 \times 10^5$ m$^2$ and a volume of $1 \times 10^6$ m$^3$. The current landslide inventory map (SAHD, 2011a) identifies 20 different sub-movements (five falls, three rotational slides and twelve complexes) within the Termini-Nerano valley, covering a total area of $4 \times 10^5$ m$^2$ (Fig. 3a). The SAHD inventory is based on a combination of aerial photography and Digital Terrain Model (DTM) interpretation complemented by field surveys. The inventory is then combined with geomorphological predisposing factors to derive the susceptibility and finally is overlaid to vulnerability and exposure information to empirically asses the risk levels following a matrix-based heuristic approach (Fig. 3b).

The LRM is therefore generated with a method based on expert opinion which, inevitably, cannot account for the many uncertainties associated with the landslide processes.

## 3. Materials and methods

The multidisciplinary approach of the work has been designed to define the relative landslide risk (R) limited to the slow-moving phenomena (Fig. 4). Different investigations have been performed to retrieve the characteristics of the landslides needed for assessing and validating R.

The geological and geomorphological information of the valley have been derived from field surveys conducted between 2012 and 2013 and then integrated with sub-surface data acquired though five boreholes

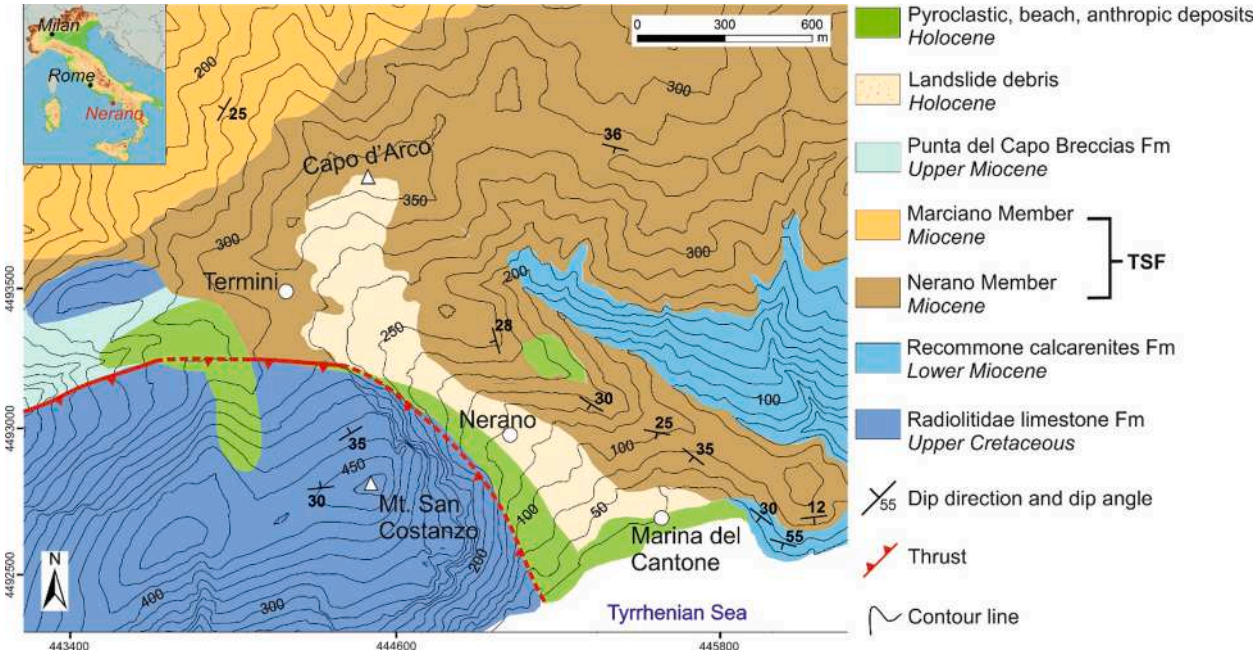


**Fig. 2.** Geological map of the Termini-Nerano area. Coordinate system: WGS 1984, UTM Zone 33N.

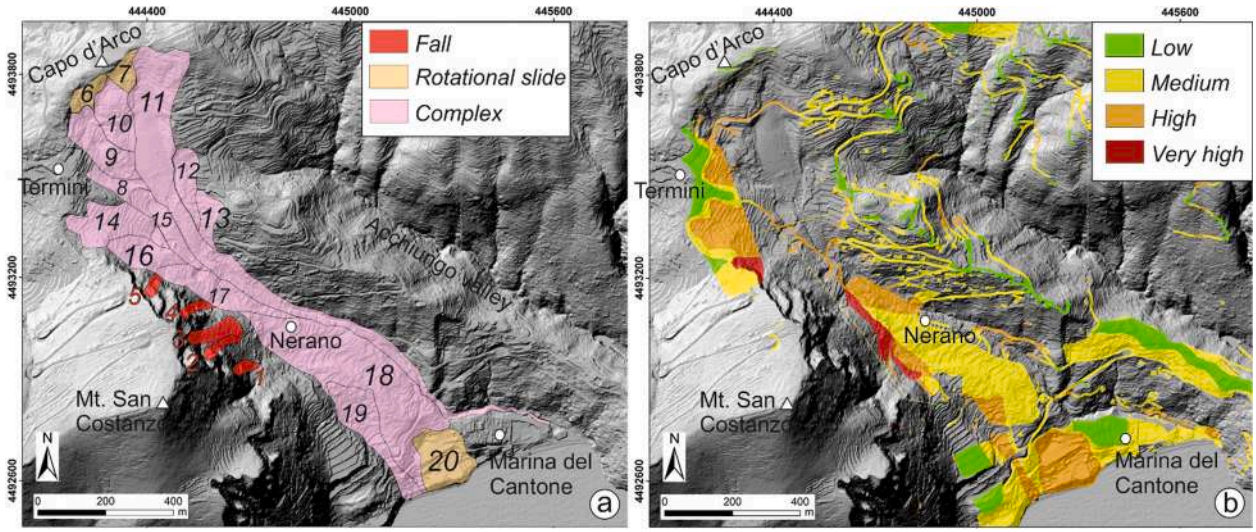


**Fig. 3.** Landslide inventory map (SAHD, 2011a) where each number refers to a single landslide classified according to the type of movement (a). LRM (SAHD, 2011b) that shows the level of risk only where infrastructure are present (b). The two maps are overlapped onto shaded relief DTM. Coordinate system: WGS 1984, UTM Zone 33N.

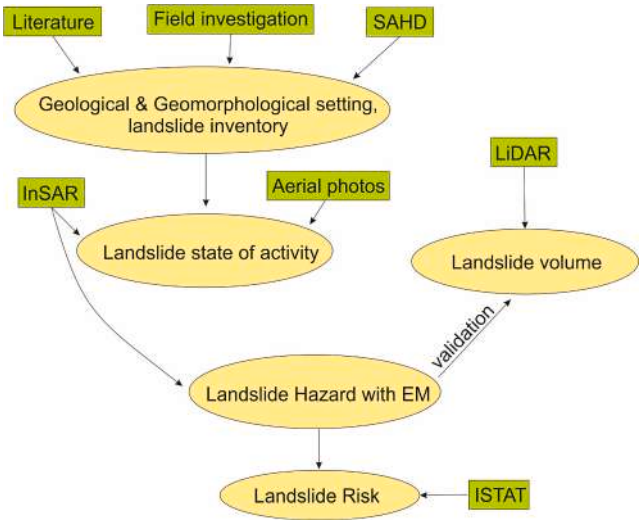


**Fig. 4.** Workflow of the approach adopted in this work. Techniques and input data are in green, outputs in yellow. Inputs data include the landslide inventory and geomorphological maps from the Southern Apennines Hydrographic District (SAHD), ground deformation displacement from Interferometric Synthetic Aperture Radar (InSAR), hazard maps from the Ensemble Modelling (EM) and exposure and vulnerability data from the Italian National Institute of Statistics (ISTAT). (For interpretation of the references to colour in this figure legend, the reader is referred to the web version of this article.)

drilled in landslides 11 and 18 where, successively, three inclinometers and two open stand-pipe casings have been installed, recording data from different sectors of the valley (Fig. 5). These investigations provided information on the type of materials involved in the instability and its kinematics, constrained the volumes associated to the active part of the landslide and validated the InSAR results.

The remote sensing dataset allowed the understanding of the state of activity of the movements, the interaction between the instability zones within the valley and the estimation of the landslide volumes. Remote sensed data include aerial stereo photographs, LiDAR DTM and InSAR velocities maps. Aerial stereo photographs for the 1955–2011 time span were obtained from the Italian Military Geographic Institute and the Agency of Agriculture, Food and Forestry of the Campania Region, the acquisitions were taken at flying heights ranging from 2,700 m to 6,200 m with a scale ranging between 1:10,000 and 1:41,000. The DTM, acquired from airborne 2012 LiDAR data, with a resolution of 1 m and root mean square error of ~0.15 m (http://sit.cittametropolitana.na.it/lidar.html), has been used to assess the original volume associated to each landslide. InSAR results have been generated from 35 ascending and 35 descending COSMO-SkyMed (CSK) X-band images acquired in the 20/10/2011–19/4/2014 and 20/2/2012–23/12/2013 interval, respectively. The two geometries have been processed at 3 m × 3 m resolution by means of the Persistent Scatterer Pair technique (PSP; Costantini et al., 2014) as part of the third phase of the Not-ordinary Plan of Environmental Remote Sensing project (Piano Straordinario di Telerilevamento Ambientale – PST-A), a nationwide monitoring plan run by the Italian Ministry of Environment and Protection of Land and Sea in cooperation with the Italian Space Agency (Costantini et al., 2017; Di Martire et al., 2017).

The EM has been trained to produce the landslide hazard (H) via three MLAs (ANN, GBM and MaxEnt) well-known for their good performance (Elith et al., 2006). ANN refers to a large group of models that are inspired by biological neural networks to process information. These networks are typically structured in layers with an input layer containing the environmental variables used to train the model, several hidden layers in which the function applies weights to the inputs and directs them through an activation function as the output (Dou et al., 2015). GBM is a ML technique for regression and classification models. GBM repeatedly perform many decision trees to enhance model precision. For each new tree in the model, a random subset of all the data is selected using the boosting method, which iteratively aims to reduce the errors of the previous one (Kim et al., 2018). MaxEnt is a "presence-only" spatial distribution method. It makes use of occurrence data and a large number of points throughout the study area, known as background points. MaxEnt calculates the ratio between two probability densities (occurrence and background points), which gives the relative "environmental suitability" for the presence of an event for each location in the study area (Sepe et al., 2019). The MLAs use predisposing factors determined and assessed from the geological, geomorphological and kinematic characteristics of the instabilities which do not show collinearity according to the Variance Inflation Factor (VIF) calculation (Arabameri et al., 2019). To perform and assess models achieved with various MLAs, the K-fold Cross-Validation (K-CV) approach was used. The latter splits a random part of the input population (~80%) for calibration while the remaining (~20%) is used for testing the

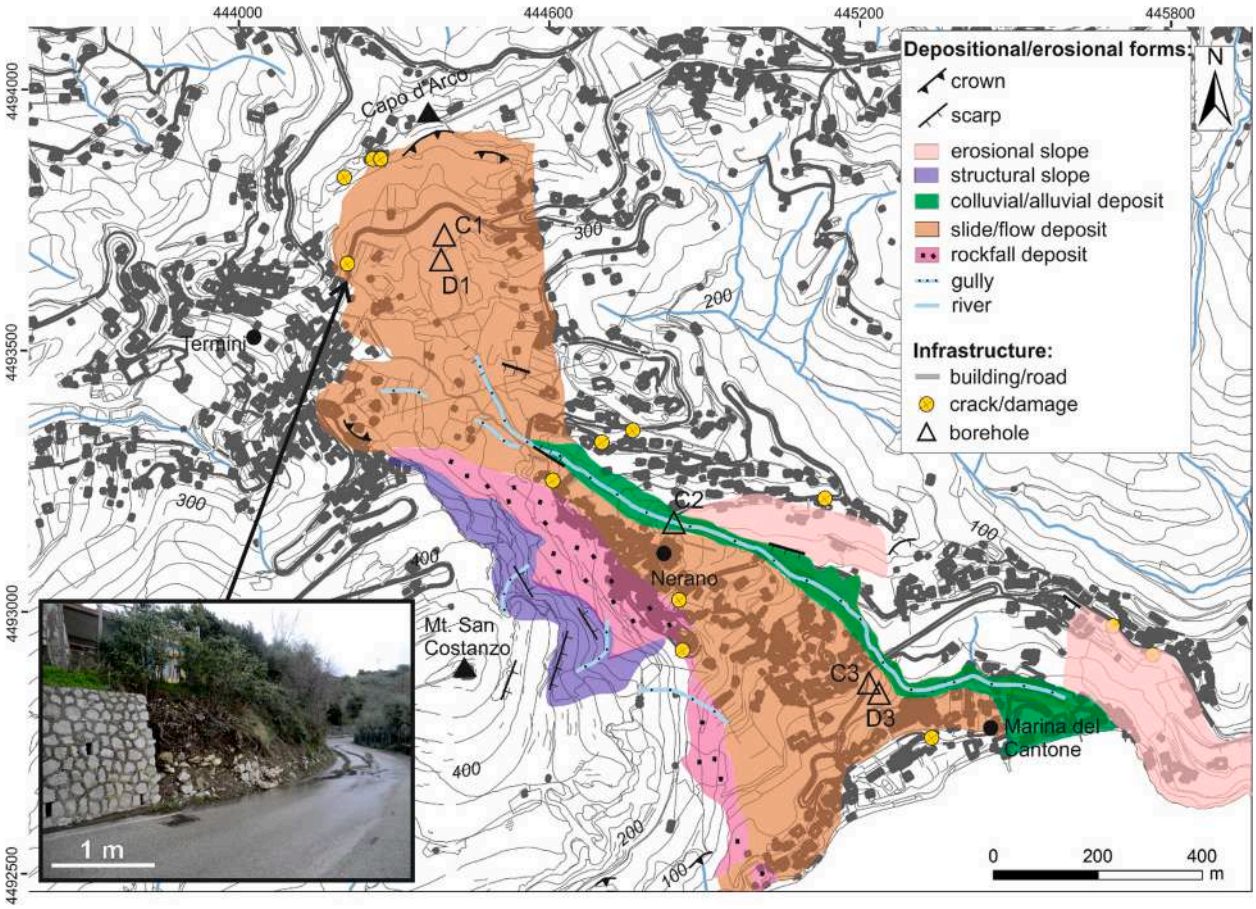


**Fig. 5.** Geomorphological map of the Termini-Nerano valley where slope and superficial deposits have been classified according to the dominant morphogenesis. Coordinate system: WGS 1984, UTM Zone 33N (modified from SAHD, 2011c).

prediction of the model; the entire approach is then replicated several times for each of the three models and the average predictive accuracy is finally reported through the Area Under the Receiver Operating Characteristic (AUROC) curve and True Skill Statistic (TSS) (Araujo et al., 2005). Afterwards, the three MLAs were ensembled and H was evaluated by considering the median values of the spatial probability of landslide occurrence from the three models. The short temporal interval of the InSAR time series, 3 years, despite provides a constrain on the state of activity of the landslides, does not provide a sufficiently long record needed to assess the return periods of the landslides which tend to be in the order of tens of years in this area (see Section 2). So the H defined in this paper is a relative hazard which does not account for the probability of landslides occurrence within a given period of time, a solution already adopted whenever the knowledge of landslide mechanisms is limited (Andrejev et al., 2017).

H has been integrated with information on local population and buildings to generate R which, similarly to H, it refers to a relative risk. Spatially, the R can be conceptually represented as a non-homogeneous Poisson process (NHPP) similarly to what has been done in Bartolini et al. (2013) when simulating different eruptive scenarios:

$$R = 1 - \exp((H + V + E)^* - 1) \quad (1)$$

where V is the degree of damage (namely the vulnerability) of a specific element-at-risk (E) inside the area. H, V and E represent variables associated to the landslide that can change in time following a non-homogeneous Poisson process with an exponential distribution. The probability density function for V and E have been calculated over the territorial units defined by the Italian National Institute of Statistics in 2011 (ISTAT, 2011) for the area of study.

## 4. Results

### 4.1. Geological-geomorphological investigations

Landslide events have intensively reshaped the superficial deposits of the Termini-Nerano valley where the intensive urban development, especially between 1919 and 1990 according to ISTAT (2011), is now partially covering geomorphological signatures of instabilities. The morphoevolution of the valley occurs prevailingly through slides and flows and secondarily by rockfalls and surface runoff through gullies (Fig. 5).

The main scarp is associated to a ~15 m high crown area and is located in the Capo d'Arco area, on a 20° slope. Downslope, landslide flow and slide deposits from lateral lobes converge and fill the structurally-controlled NW-SE valley. Despite the anthropogenic disturbance, which has confined gullies on the eastern side of the valley, scarps in the order of some meters are still preserved in the landslide deposits within the catchment area. Gullies transport colluvial and alluvial deposits along a NW-SE direction which take a 90° bend downslope, just north of Marina del Cantone, where have been removed by human intervention to allocate space for leisure activities. On the western side of the valley, the mass movement deposits are topped by coarse-grained rockfall material from Mt. San Costanzo but are also embedded in the flow and slide deposits (Fig. 5).

The lithology of landslides 11 and 18 and its relationship with the bedrock was determined from drillcores (see Fig. 3). The superficial units are mainly characterized by alternating beds of shales, silts, sandstones and, in the transport and accumulation zones, calcarenitic-sandstones from the marly-calcareous olistoliths of TSF (Fig. 6). The

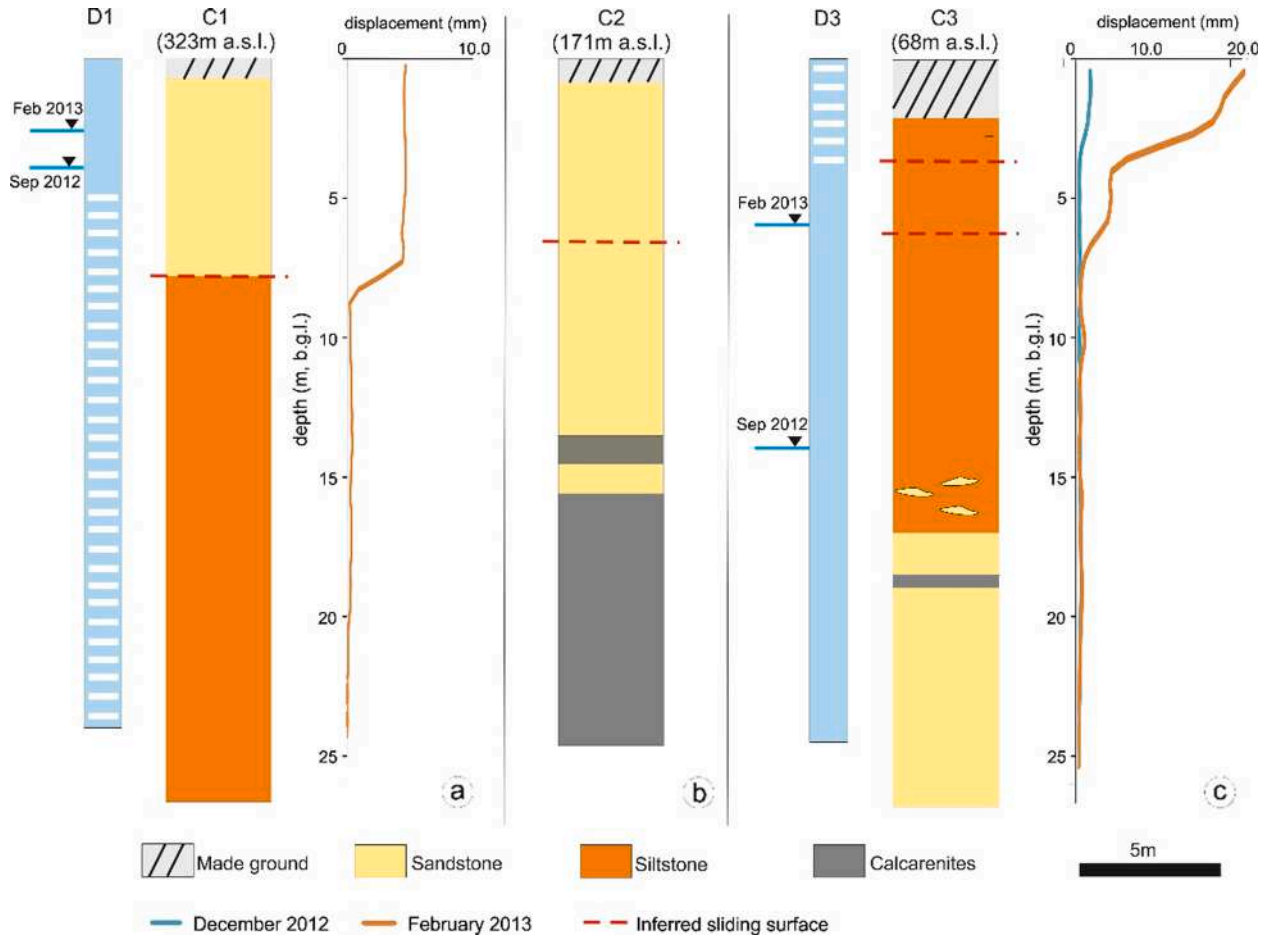


**Fig. 6.** Sketch showing the stratigraphic logs of the units investigated. Piezometers installed are represented in blue with white stripes indicating the screened section of the borehole. Inclinometer's zero reading: September 2012. Location of the boreholes is provided in Fig. 5. (For interpretation of the references to colour in this figure legend, the reader is referred to the web version of this article.)

component of clay minerals, determined from laboratory grain-size analyses, increases from 10% wt. in C1 to 20% wt. in C2 and 30% wt. in C3 (Cesarano et al., 2018).

The shallower layers of superficial material are composed of poorly cemented sandstone or siltstone levels with different degree of weathering and heterogeneity with depth, so confirming the presence of overlapping mass movement deposits above the bedrock, the latter only found down to 20 m in C3 (Fig. 6). We have indeed interpreted the calcarenites levels in C2 as one of the exotic block embedded within the TSF, being the Recommone Calcarenites Formation at ~100 m depth in this location.

Inclinometric data show a single slip surface at around 8 m depth in the upper part of the slope (C1) with displacements of ~5 mm, and two slip surfaces in C3, at depth of 4 m and 6 m, with displacements decreasing downwards and an overall disarranged structure down to ~20 m. No reliable information could be reported from C2 as the aluminum casing broke at ~6 m b.g.l. soon after its installation, suggesting at least one slip surface at such depth. These differences in the borehole lithology and the measured inclinometric-material response play an important role in understanding the kinematics of landslide 11 which is characterized by plastic deformation in the head area with a motion similar to a slide which becomes a creep downhill where the clay fraction increases and the failure surface is not so clear anymore.

Groundwater levels, measured from September 2012 to February 2013, suggest the occurrence of an unconfined shallow aquifer located in the fractured mass above the slip surface which has different characteristics in the crown and the toe area given the different response in groundwater rise (~1 m in D1 and ~3 m in D3) for the 932 mm of rainfall occurred over this time interval.

### 4.2. *Aerial photography stereoscopic analysis*

The oldest aerial photos available, dating back to 1955, show sparse vegetation and extensive outcrops of the TSF. The four main lobes belong to the 1941 landslides east of Termini that had developed into a flow which had reached the village of Nerano and spread as soon as it reached the Marina del Cantone village (Fig. 7a). The three main lobes correspond to the crown sectors of landslides 9, 10, 11, 14 and 15 of the SAHD landslide inventory map (see Fig. 3a). The 1974 aerial photograph highlights remedial works carried out by the Public Works Department of Naples following the 1963 landslides which led to the construction of retaining walls and drain trenches connected to a drainage basin downslope (Fig. 7b). The imagery shows that the 1963 event developed in the eastern sector of the Capo d'Arco hill, within the 1941 deposits, had an aerial extension ~30% smaller than the previous event and was diverted almost at a right angle nearby the Marina del Cantone village possibly by the 1941 toe zone, which might have confined the flow towards the eastern side of the valley. The following bioengineering interventions allowed a pine forest to develop on the surface of the 1963 landslide body, which matured in the following years, as evident from the 1990 frames (Fig. 7c). From 1990 onward, the intense urbanization of the area erased any geomorphological evidence of the older landslides with vegetation wiped out by fall and topple deposits generated from the eastern side of Mt. San Costanzo, sometime between the 70s and the 80s.

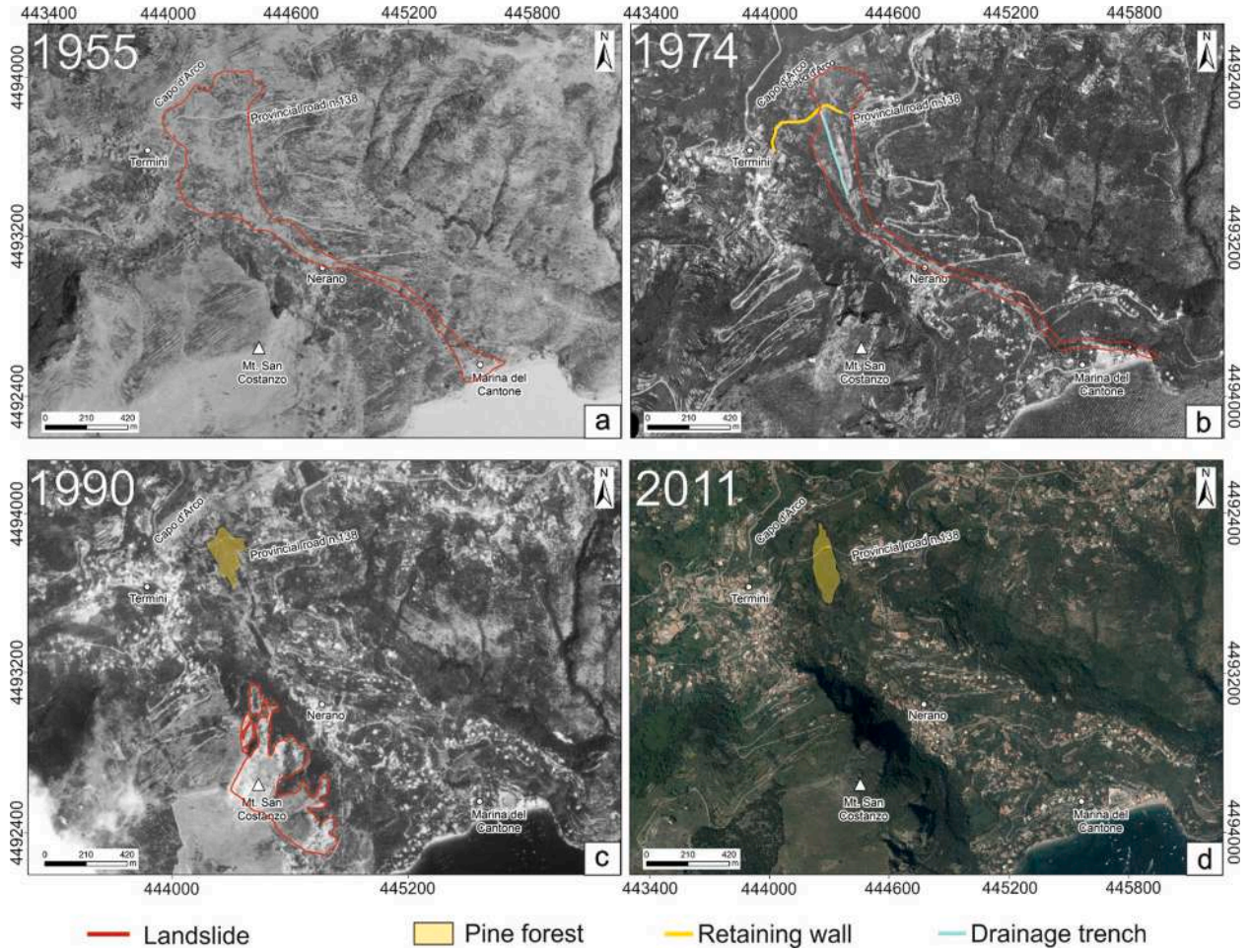


**Fig. 7.** Inventory of the active landslides within the Termini-Nerano catchment from aerial stereo-photos: 1955 (a), 1974 (b), 1990 (c), 2011 (d). Coordinate system: WGS 1984, UTM Zone 33N.

In 2011, the intense urbanization of the area erased any geomorphological evidence of the older landslides (Fig. 7d).

The 1941 and 1963 event geometries control the following development of any smaller landslides between Capo d'Arco and Nerano that remobilise material from the past landslides. However, their slow velocity and dimensions do not provide scars identifiable in the stereo-photos but still observable on the field, such as the damage associated to landslides 6 and 7 and representing the retrogressive evolution of the landslides system (see Fig. 5).

### 4.3. LiDAR analysis

The 2012 DTM has been used to reconstruct the pre-landslides (original) topography, retrieve the vertical differences between the current and original topography and then assess the volumes. The original topography has been defined by using as reference surface the topography from un-failed portions of the slopes. The reconstruction is based on three assumptions: the unslided wallslopes represent the original geomorphology of the area had the landslides not occurred (i), the sediment transport process, from sediment detachment to its depositions only occurs within this catchment (ii) and that human reprofiling (e.g., terracing, embankments) of the slope has had a limited impact on the elevations despite the wide urbanisation of the valley (iii).

The reconstruction has considered linear, exponential or logarithmic functions to perform a 1D fitting for profiles along and across the valley, similarly to what has been done in Chang et al. (2018). Of the three regression functions applied to each profile, the one with the highest coefficient of determination ($R^2$) has then been selected. A total of 41 profiles parallel and orthogonal to the landslides and within the TSF have been considered (Fig. 8a):

- Five profiles parallel to the direction of motion of the landslide bodies, to represent the original topography along the main direction of the valley. These profiles have been derived from the regression of five profiles located outside the Termini-Nerano valley, in the northern facing slope of the Sorrento Peninsula (Fig. 8b). These sections have been chosen as they are largely unaffected by tectonic processes, human activities (terracing, re-profiling) and previous mass movements and have a similar elevation range to the Termini-Nerano valley. The best model retrieved from the five profiles outside the landslide areas has then been used to retrieve the pre-landslide longitudinal profiles along four profiles within the Termini-Nerano valley and parallel to the main direction of motion.
- Twenty-seven profiles transverse to the landslide bodies, to represent the original topography across the main landslides pathways. In this case the west and east side of the Termini-Nerano valley that bound the eastern and western side of the landslide bodies have been fitted by the models independently (Fig. 8c). Again, the transverse profiles were reconstructed by selecting, every time, the regression with the highest $R^2$.

An envelope surface has been subsequently interpolated from the 31 profiles by using the Inverse Distance Weighting (IDW) method. The average $R^2$ value of 0.83 from the best fitting models along the profiles

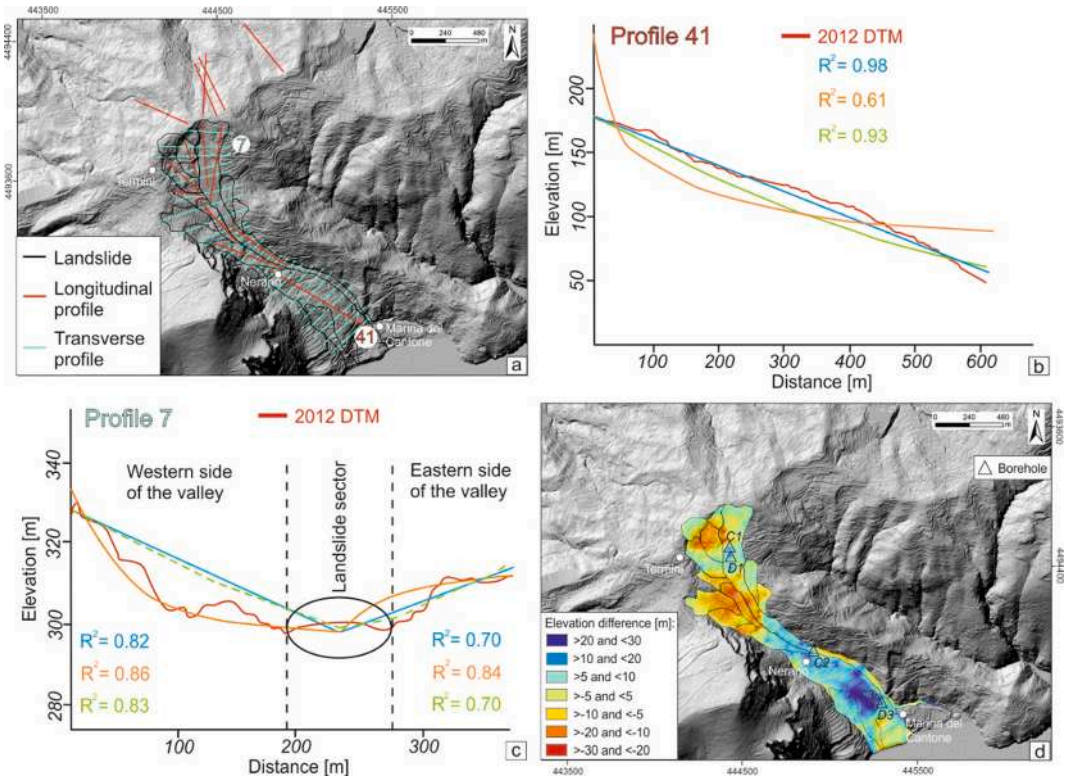


**Fig. 8.** Location of the longitudinal and transverse profiles overlapped onto the hillshade map of the study area obtained from the LiDAR DTM (a). Example of the regression model for the longitudinal profile number 41 (b) and the transverse profile number 7 (c) where blue, orange and green colour refer to the linear, logarithmic and exponential fitting, respectively. Elevation difference between the 2012 DTM elevation and the reconstructed topography where positive values indicate accumulation areas and negative values indicate depleted areas (d). (For interpretation of the references to colour in this figure legend, the reader is referred to the web version of this article.)

supports the idea that, especially in the narrow parts of the valley with steeper surfaces, the envelope surface can be considered an optimal way to reconstruct original topography.

Compared to the actual morphology, the envelope surface reveals a more rugged topography in the crown area and a gentler slope at the bottom of the valley (<10° vs 20/30°). The depletion/accumulation map could finally be retrieved from the vertical difference in the elevations between the 2012 topography and the reconstructed topography (Fig. 8d).

Positive differences mean that the 2012 topography is above the original topography (i.e. accumulation areas) while negative differences indicate that the 2012 topography is below the original topography (i.e. depleted areas) as a result of the mass movements.

DTMs difference highlights two depletion areas, one spreads across the crown sectors of landslide 9, 10 and 11 and the other one where the mass deposits direction of flow converges in the narrow valley between Termini and Nerano (landslide 15 and 17), in this part elevation difference is −27 m. The accumulation area is instead located southward, between Nerano and Marina del Cantone, where the 2012 topography is 31 m higher than the reconstructed one. Vertical differences are usually 10 m lower than slip surfaces retrieved from the inclinometers, thus supporting the idea that the current moving landslides just involve the superficial deposits of the whole landslide mass.

By taking into account the area, vertical differences have been converted to volumes for each landslide. The volume differences prove that landslides 17, 18, 19 and 20 represent net accumulation areas while all the other landslides have a net mass loss. The spatial extension of landslide 11, from the crown to the toe, inevitably encompasses multiple areas of depletion and accumulation.

The whole displaced mass amounts to ~$1.484 \times 10^6$ m$^3$, (Table 1).

Because historically small landslides within the Termini-Nerano valley develop within the older deposits, is likely that reactivations will be fed by materials located southeast of Nerano, especially at the steep eastern edge of landslide 18 where a net accumulation sector has formed. Considering the positions of the sliding surfaces measured at C1, C2 and C3 within landslide 11 and 18, we can estimate that a volume of at least ~$0.67 \pm 0.03 \times 10^6$ m$^3$ is currently active.

**Table 1**
Area, average elevation difference and volume gain/loss for each rotational and complex landslide in the Termini-Nerano valley.

| Landslide ID | area [m$^2$] | net volume difference [m$^3$] |
|---|---|---|
| 6 | 11,931 | −32,620 |
| 7 | 6,214 | −38,181 |
| 8 | 7,637 | −90,562 |
| 9 | 21,387 | −101,827 |
| 10 | 17,932 | −235,681 |
| 11 | 100,284 | −89,503 |
| 12 | 11,975 | −19,299 |
| 13 | 8,093 | −55,820 |
| 14 | 25,427 | −332,216 |
| 15 | 14,780 | −279,220 |
| 16 | 14,768 | −201,408 |
| 17 | 22,603 | 7,974 |
| 18 | 95,448 | 1,245,974 |
| 19 | 25,471 | 234,569 |
| 20 | 24,003 | 4,298 |
| *Total* | *407,954* | *16,477* |

### 4.4. InSAR analysis

InSAR measurements have been used to characterize the slope kinematics. By taking into account the standard deviation (σ) of the LOS

(Line of Sight) velocities such as in Aslan et al. (2020), the stable target threshold has been set to ±1.5 mm/yr, ~2 times σ. The results reveal the presence of many areas still affected by surface displacements along the basin and related to active slope instability phenomena with the presence of vegetation that hinders the density of radar targets.

CSK results (Fig. 9) for the period 2011–2014 have a density of ≥1,800 targets/Km$^2$ and highlight that seven mass movement systems are moving with instability confined to the head (landslide 6 and 7) and the toe areas (landslides 11, 17, 18, 19 and 20) where LOS velocities reach 10 mm/yr in the descending geometry. A poor targets coverage characterises the landslides between Termini and Nerano but, based on geomorphological and ISBAS data, we can realistically assume that none or limited motion occurs here.

Where CSK radar targets were sufficiently covering displacing masses (landslides 11, 17, 18, 19 and 20), the ascending and descending LOS displacements have been projected along horizontal and vertical directions after interpolation through the IDW method and application of Dalla Via et al. (2012) method. The derived time series have been averaged in time, considering the closest satellite acquisitions, and in space, considering the same landslide body identified from field surveys, in order to be compared with the monthly rainfall record of the area available from the Massa Lubrense raingauge station, located ~3 km northwest of our study area.

Following Bonì et al. (2018) classification method for the InSAR time series, the temporal analysis reveals that landslides move seasonally (non-linearly) with acceleration during Winter months and deceleration in Summer months and a time lag of 2–4 months with the precipitation peaks (Fig. 10). This temporal heterogeneity is more evident for the horizontal motion. While the geometry of the large mass events controls the development/reactivation of smaller rotational and complex landslides within the valley (see Section 4.2), InSAR time series analysis reveals that seasonal stress perturbations control the magnitude of the motion rates at a short temporal scale.

Finally, C1 and C3 inclinometers data have been used to validate the nearest PSP points available for the same time interval (Table 2) after the InSAR horizontal and vertical components of displacement have been spatially interpolated. The lack of a PSP in correspondence of each inclinometer might explain the tiny differences between the two measurements that overall agree and confirm the highest deformation rates at the toe of landslide 18. The latter represents an unstable body where nearly 30 m of materials have been piled up collecting deposits transported within the whole Termini-Nerano valley.

### 4.5. Landslide hazard mapping

Fourteen environmental variables considered as predisposing factors have been selected to produce H: slope angle, slope aspect, profile curvature, planform curvature, Topographic Wetness Index (TWI), Topographic Position Index (TPI), InSAR horizontal velocity (according to the interpolation shown in Section 4.4), elevation, distance to stream, distance to road, stream density, road density, lithology and land-use. A more detailed description of these is given in Supplementary 2.

Apart from InSAR displacements, the selected environmental variables represent standard factors for landslide hazard mapping (Van Westen et al., 2008). To maintain the temporal consistency of all the input datasets, only the interpolated horizontal InSAR data from CSK have been used (see Section 4.4) in combination with the LiDAR-derived geomorphological indicators and the outcropping layers mapped during our field investigations. All the layers are raster (including the InSAR results after the interpolation) that have been interpolated and brought to the same spatial resolution (10 m) and extension. Considering the (i) assumption made for the volume calculation in Section 4.3, the vertical differences from the original topography could not be used as training layer but for validation purposes only, being limited to the landside areas.

Each stand-alone model (ANN, GBM and MaxEnt) was executed with 50 different combinations of training and testing of the data using the K-CV approach (Fig. 11a-c). Such a method allows to generate 150 different H scenarios with corresponding errors values and evaluation scores (Supplementary 1). In the ensemble procedure stand-alone models with a threshold >0.7 for AUC and 0.6 for TSS only were selected. In this way, in the aforementioned procedure were chosen only the models with a good performance. The median of the probabilities of the three models has been chosen as the ensemble technique to obtain the final landslide susceptibility map, being the median less sensitive to outliers than the mean. The final ensemble map has an AUROC value of 0.96 and a TSS value of 0.82 (Fig. 11d).

The values of H, and later of E, V and R as well, have been grouped into four different classes to adhere to the Italian laws on hazard and risk assessment. The natural breaks method has been chosen to divide the distribution in these classes so to minimize the variance within each class and maximizing the variance between the classes (Fig. 11).

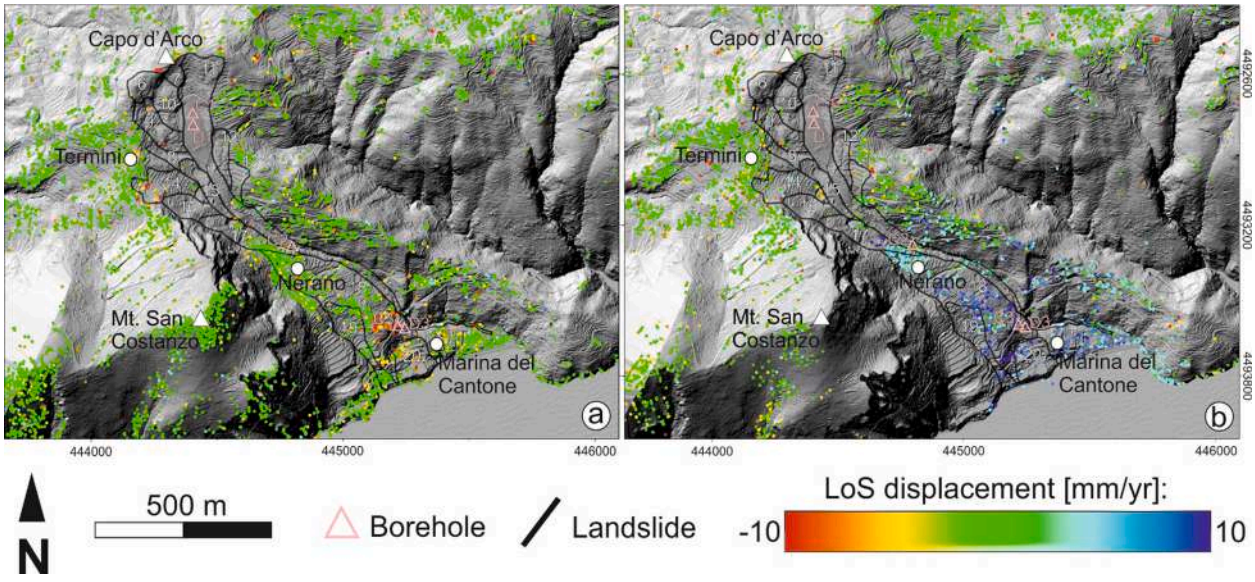


**Fig. 9.** InSAR displacements along the LOS obtained from the CSK ascending (a) and CSK descending (b) data. Positive numbers correspond to motions towards the sensor, negative ones to motion away from the sensor along the LOS. Coordinate system: WGS 1984, UTM Zone 33N.

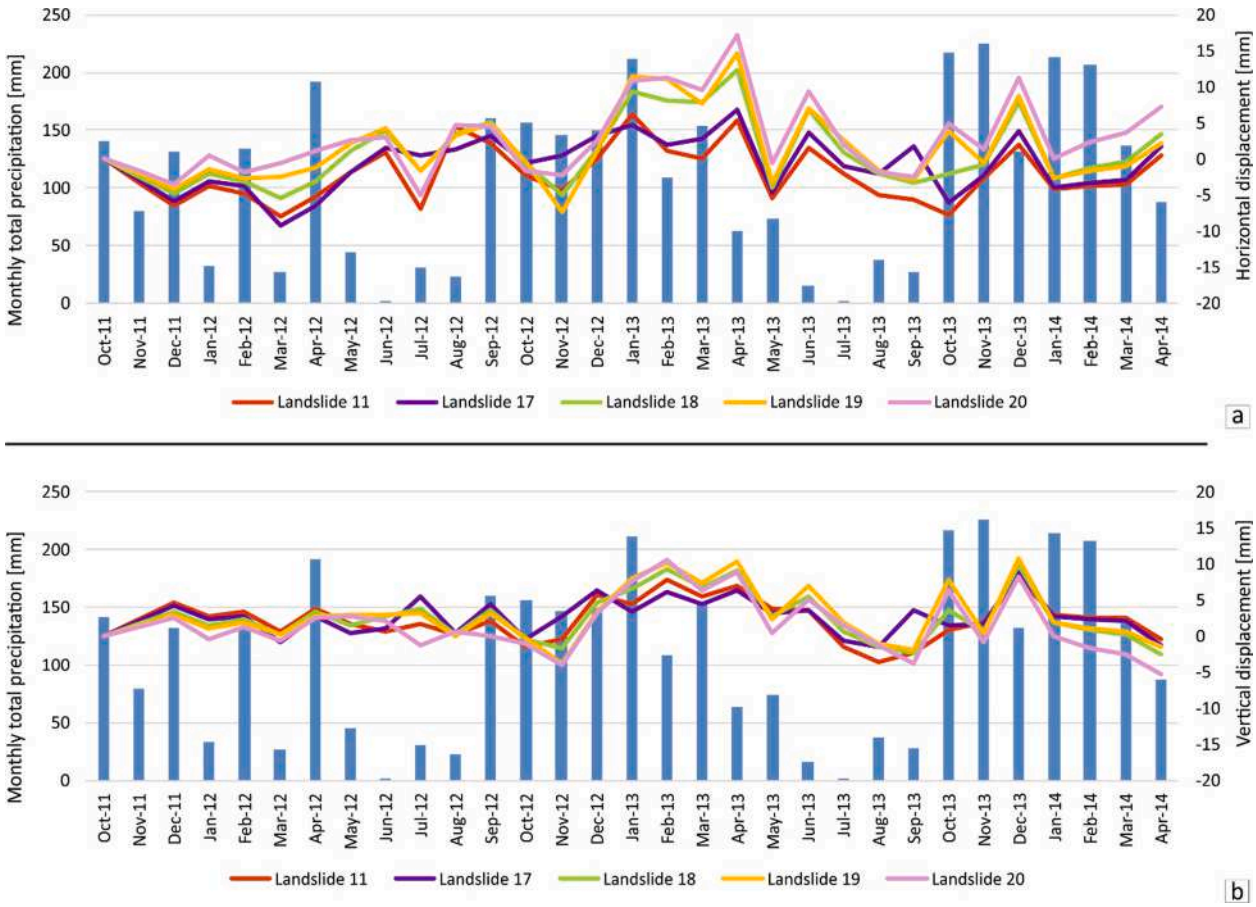


**Fig. 10.** Average displacements for landslides 17, 18, 19 and 20 projected along the horizontal (a) and vertical (b) direction. Blue bars indicate monthly total precipitation. (For interpretation of the references to colour in this figure legend, the reader is referred to the web version of this article.)

**Table 2**
Comparison between inclinometer and interferometric data. For the borehole location, see Fig. 9.

| Inclinometer | Period of acquisition (m/yyyy) | Inclinometer displacement (mm) | Inclinometer azimuth (°) | InSAR displacement (mm) | InSAR horizontal displacement (mm) |
|---|---|---|---|---|---|
| *C1* | *9/2012–2/2013* | *5.0* | *140 (SE)* | *1.5* | *3.9* |
| *C3* | *9/2012–2/2013* | *20.0* | *180 (S)* | *10.7* | *14.3* |

EM shows that the highest hazard is located on the northwestern sector at the toe of the landslide system with only landslides 6, 10, 12, 13 and 15 presenting a low to medium risk. On the other hand, whole landslide bodies (18, 19 and 20) show a very high hazard. Additional hazard is posed by the bottom of the Mt. San Costanzo eastern slope. Score values, between 0 and 1, indicate how the factors in EM contributed to H (Table 3). It has to be highlighted that we have not considered interactions between variables so every factor has been examined independently. Scores close to 1 greatly affect H while values close to 0 have no influence on the landslide hazard. Three main predisposing factors emerge: horizontal displacement, slope aspect and the road density.

InSAR displacement is the most influential factor, highlighting the importance of regularly monitoring such type of landslides for building a reliable H. Consequently H tend to be higher where velocities are the greater. The south facing aspect is an important factor especially if considered with respect to the attitude of the TSF strata whose dip directions converge toward the Termini-Nerano valley. Indeed, over the north facing slope just north of Capo d'Arco, no landslide is reported.

Road density is acknowledged to be a predisposing factor especially in the centre of Nerano, where narrow scenic road snakes within the village, but not a triggering factor since there is no temporal relationship between the road works and the occurrence of the landslide. Lithology is not a predominant predisposing factor as the largest contrast in the mechanical and structural properties, according to the borehole data (see Section 4.1), lies within the different landslide deposits developed in the same unit, the TSF. Similarly, slope angle has a low influence on H since slow-moving landslides in SCFs can develop and move on low angle slopes (<10°), flat, or even slightly uphill terrains (Del Soldato et al., 2018).

### 4.6. Landslide risk mapping

The LRM has been combined with information on its potential impact which is expressed by E and V. The latter have been sampled by ISTAT over six different units (Fig. 12). These units do not correspond to administrative or geomorphological boundaries but follow the guidelines of Regulation (EC) no. 1059/2003 of the European Parliament on the establishment of territorial units that can be used for statistical analyses of population and buildings across Europe.

Exposure information has considered information on the number of residents and building within the territorial unit.

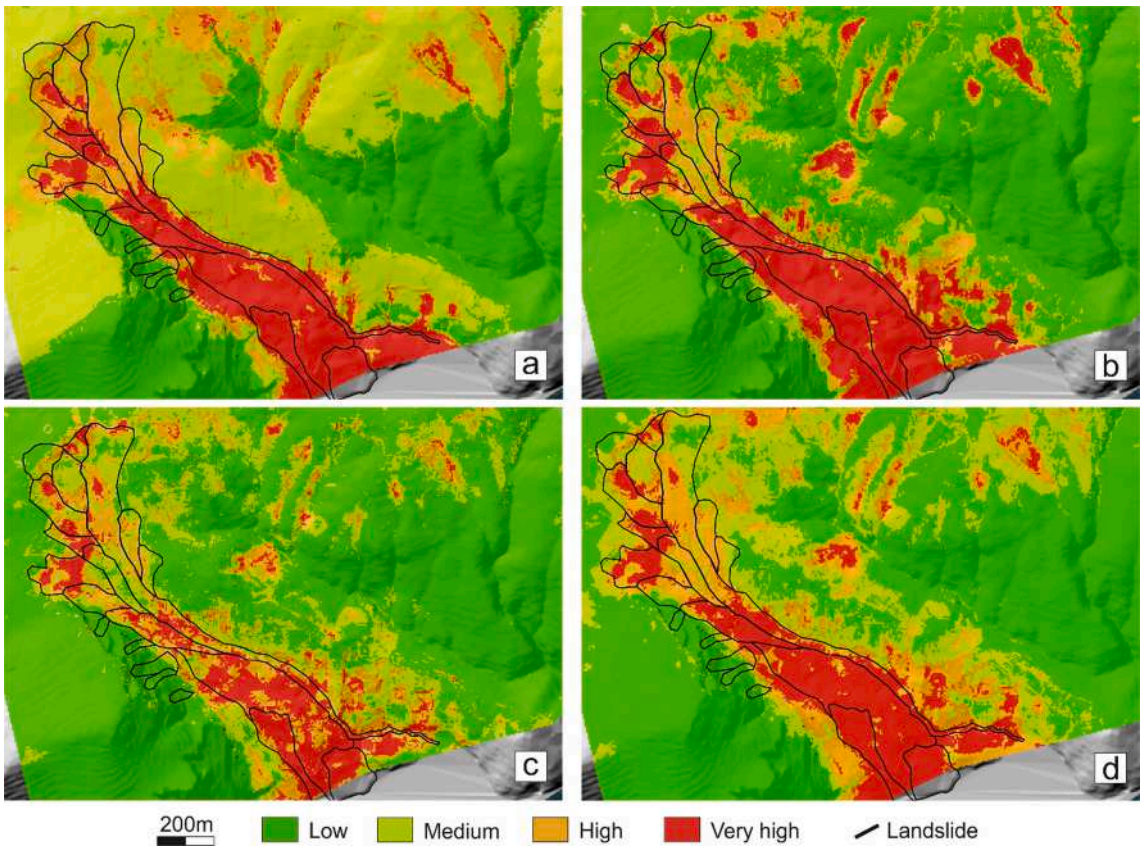


**Fig. 11.** Median value of the hazard map from 50 ANN runs (a), from 50 GBM runs (b) and from 50 MaxEnt runs (c). EM landslide hazard map considering median values from the 50 ANN, 50 GBM and 50 MaxEnt models (d).

**Table 3**
Scores of the fourteen variables used in the EM.

| Factor | Score | Factor | Score |
|---|---|---|---|
| Distance to road | 0.042 | Profile curvature | 0.01 |
| Distance to stream | 0.008 | Road density | 0.136 |
| Elevation | 0.037 | Slope angle | 0.025 |
| Lithology | 0.03 | Slope aspect | 0.144 |
| InSAR displacement | 0.237 | Stream density | 0.055 |
| Land-use | 0.001 | TPI | 0.027 |
| Planform curvature | 0.029 | TWI | 0.009 |

Given the different size of each territorial unit, the density of buildings and population has been considered for E (Table 4). ISTAT does not provide information on the road network, so this information has been excluded, but it would spatially represent a minor component of the infrastructures here. About V, since most of the buildings are masonry and other types of buildings (concrete, steel and wooden) represent <0.2% of the urban fabric, only the buildings age has been considered as a discriminant component for V.

V and E have then been normalized and summed to H according to the formula given in (1) and the LRM has been generated (Fig. 13a). R values range between 0 (low risk) and 1 (very high risk) and have been reclassified according to the natural breaks criterium. The low standard deviation (0.09) compared to the ranges of each class of R into a high precision for our map (Fig. 13b).

According to the LRM, most of the valley is under medium and high risk with the highest risk located south of Termini and in the bottom part of the valley, where most of the recorded damage has been mapped (see Fig. 5). The very high risk southeast of Termini and on the eastern side of the Termini-Nerano valley is associated to the high population density and old building age while the very high risk in Nerano is mainly due to H despite the lower population density (E) and relatively younger buildings (V). In turn, the very high H in Nerano is mainly due to InSAR displacement. A medium to high risk is instead characterising the top of the valley as result of the low density of population and buildings in those territorial unit.

## 5. Discussion

The Termini-Nerano valley has been chosen as test area for developing a new methodology to assess landslide risk due to the range of datasets available. The latter has allowed to build a multidisciplinary approach which provides a holistic understanding of the landslide risk in the catchment where, in the meantime, local population has lost the historical memory of the landslides activity (more than a generation) and so underestimate the current risk.

In the studied area, geological and geomorphological observations have identified fifteen extremely-slow-moving landslides, according to the Cruden and Varnes (1996) classification scheme, covering a total area of $4.1 \times 10^5$ m$^2$.

Field mapping reveals that one of the most important controlling factors for landslides susceptibility is the lithology given by the dip-slope attitude of the TSF layers and its role for the geometrical distribution and evolution of the instabilities. Indeed, the valley evolution is characterised by large and catastrophic movements, like the 1941 and 1963 with velocities up to m/h, who redistribute large volumes of material from the TSF. Between these big events, however, the slope is continuously reshaped by smaller instabilities that mainly redistribute the material within the toe area. We retrieved the volume of each landslide deposit from the LiDAR-reconstructed topography and estimate a total volume of ~$1.484 \times 10^6$ m$^3$ for the whole landslides system. The net mass increase ($0.016 \times 10^6$ m$^3$) represents ~1% of the total volume calculation and can be attributed to: errors in the regression and

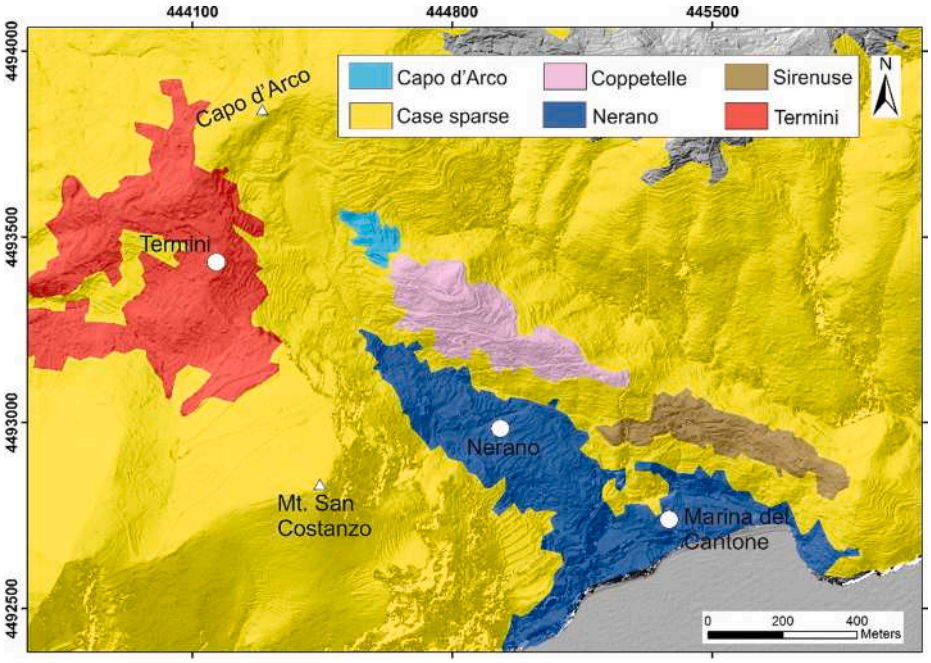


**Fig. 12.** Territorial units defined by ISTAT for the Termini-Nerano area.

**Table 4**
Main indicators used to extract element-at-risk and vulnerability inside the Termini-Nerano valley according to the ISTAT territorial units (see Fig. 12).

| | | | *density of buildings constructed in time* | | | |
|---|---|---|---|---|---|---|
| Territorial Unit | population/km$^2$ | buildings/km$^2$ | <1945 | >1946 & <1970 | >1971 & <2000 | >2001 |
| Capo d'Arco | 1,725 | 1,150 | 431 | 288 | 431 | 0 |
| Case sparse | 114 | 29 | 8 | 6 | 11 | 5 |
| Coppetelle | 2,331 | 802 | 246 | 182 | 310 | 64 |
| Nerano | 1,488 | 751 | 273 | 341 | 133 | 4 |
| Sirenuse | 688 | 398 | 15 | 260 | 122 | 0 |
| Termini | 2,255 | 754 | 278 | 172 | 260 | 44 |

interpolation method, topographic reprofiling from anthropogenic activities and contamination of fall deposits from Mt. San Costanzo. InSAR results prove the correlation between ground motion and precipitation with seven mass movements that can be still considered active but with an intermittent activity, a typical characteristic of landslides in heterogeneous terrains, such as the SCF, characterised by a long activity history with continuous reactivations (Milillo et al., 2014).

A longer record and more dense groundwater observations are needed to fully understand the hydrogeological conditions of the area such as the different response in groundwater rise observed in D1 and D3. InSAR data confirms the correlation between rates of motion and precipitation. A longer record of InSAR data, such as the inclusion of 7 years' worth of data from the Sentinel-1 constellation, would provide additional information to constraint the return period of the slope instabilities. Despite several engineering drainage solutions have been erected in the head area during the 1960s to mitigate the landslide hazard, InSAR displacements reveal that they have not been effective in stabilizing the slope. The updated landslide inventory map, InSAR displacements, land cover map and geomorphometric parameters have been used for the hazard assessment. Although several MLAs methods have been explored for the spatial-temporal prediction of landslides (Thai Pham et al., 2019), EM still represents a novelty and mainly limited to rapid or shallow landslides (Carotenuto et al., 2017). In this work we have taken a step forward and used EM for assessing the landslide hazard of slow-moving phenomena. Critical for the accuracy of EM is the selection of training points and input layers (Micheletti et al., 2014). Ideally, training points are selected over clearly identifiable landsliding areas, such a task can be relatively challenging in slow-moving landslide which might not show signs of instabilities unless a detailed field survey is carries out. Another important benefit of the landslides system in the Termini-Nerano Valley is that we could chose training and validation pixels from different landslides within the same valley thus to avoid unrealistic overestimations of prediction accuracy when training and validation points belong to the instability. In our EM we include InSAR displacements among the input layers, being velocities the only dynamic information needed to derive a hazard rather than a susceptibility map. The use of InSAR as input for improving or refining susceptibility/hazard model is not rare (e.g., Carlà et al., 2016; Ciampalini et al., 2016) but equivalently, InSAR can also be seen as a validation tool of such models especially when data available is scarce. However, in this work we considered ground motion as a predisposing factor, based on the idea that landslides in SCFs have a long reactivation history and therefore catastrophic/sudden failures always affect sectors previously unstable. Whether is training or validation, the uneven distribution of InSAR targets with a lower density over vegetated areas is a critical aspect. In such case, interpolation methods can mask or amplify ground displacements. The advent of novel InSAR processing techniques, such as the Intermittent Small Baseline Subset (ISBAS, Cigna and Sowter, 2017) or SqueeSAR (Ferretti et al., 2011), offer the possibility of filling this gap by increasing the density of InSAR measurements.

Out of the fourteen layers used for the hazard map, ground displacements is the dominant one so, even if they are considered slow-moving landslides, velocity still remains critical parameters that need to be included and regularly updated for hazard and risk calculations as

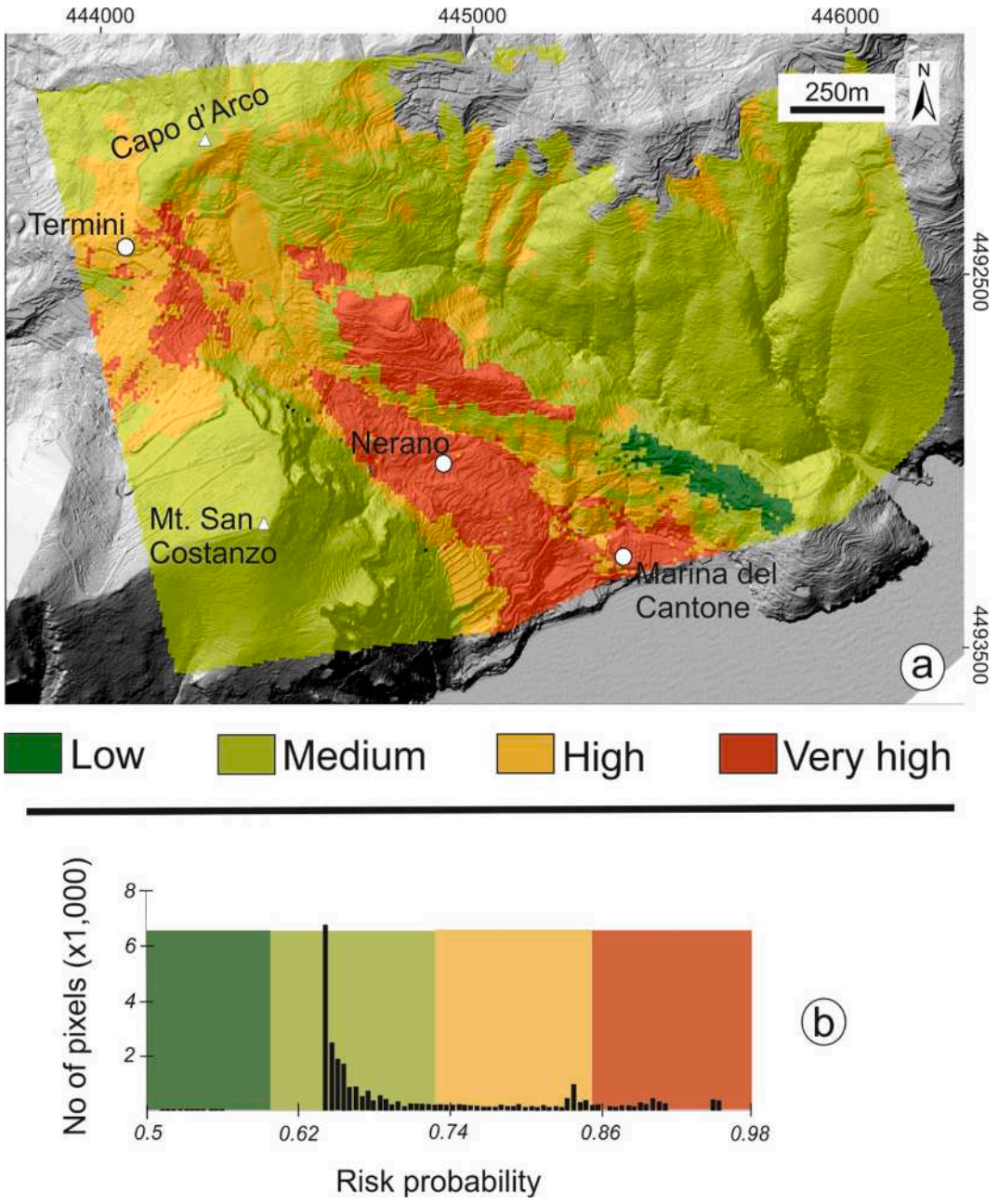


**Fig. 13.** Landslide Risk Map for the Termini-Nerano valley (a) and corresponding histogram (b).

already acknowledge in previous works (Casagli et al., 2016).

We used the vertical differences derived from the LiDAR DTM to validate the landslide hazard map. The comparison shows that the areas with very high risk corresponds to areas with the vertical differences are either highest (between Nerano and Marina del Cantone) or lowest (south of Termini).

Accumulation areas indeed are the fast-moving part within the valley with the old landslide deposits that have historically supplied unstable materials for rapid events during the 20th century. On the other hand, we interpreted the already depleted areas to be still unstable given the combination of the slope aspect, slope angle and planform curvature for these exposed landforms.

Despite the highlighted limitations, we have a unique collection of data sufficient to improve the current LRM for three reasons: updated information on the geometry and kinematic of the instabilities, a combination of three MLAs for H and the different age of the buildings has been considered for V.

Compared to the SAHD, our LRM define, overall, a more dangerous scenario where the area nearby Nerano and Marina del Cantone from a low to medium level are now classified as a high-risk level and the highest level of risk is now corresponding to areas south of Termini and on the eastern side of the valley. Field surveys confirm damage to roads and walls within these sectors. The highest difference with the SAHD LRM is over the eastward facing slope of Mt. San Costanzo because we did not account for the hazard associated to falls and topples affecting the Radiolitidae limestone Formation being it beyond the scope of this work. We have used a standard approach to evaluate R by providing the same weights for H, E and V. This, inevitably has penalised the amount of information within H which is a pixel-based layer compared to V and E that, on the other side, is a polygon-based census unit. Considering the amount of geological, geomorphological and kinematic conditioning factors which have been ingested in the risk assessment calculations, some of them with nonlinear distributions (e.g., InSAR data, E and V), single statistical or ML methods can easily bring to completely different

risk scenarios. These standalone maps can show large discrepancies especially when are compared against each other, have to be updated or upscaled (Jacobs et al., 2020). On the other side, EM has enhanced the power prediction of individual classifiers while decreasing noise and over-fitting problems by combining different MLAs together.

## 6. Conclusions

Assessing landslide risk is one of the highest challenges in land management and is usually delegated to national institutions such as geological/environment surveys, civil protection agencies or the River Basin Authorities in the case of Italy (Solari et al., 2020). Better risk assessment would support the development of strategies towards disaster risk management and disaster risk reduction. As landslide activity is expected to grow worldwide as a result of a changing climate (Gariano and Guzzetti, 2016), the capacity to timely and properly predict landslide susceptibility is critical. The current study contributes to the advancement of landslide risk analyses. Indeed, an innovative methodology for producing LRMs, with the combination of InSAR and EM, has been developed and implemented over the Termin-Nerano landslides system where we could complement standard field surveys and geological investigations with different remote sensing data.

The exploitation of MLAs is still in its infancy, far away to become a standard practice to support researchers, public entities, authorities and civil protection agencies which have the mandate to generate landslides risk mapping. However, under the pressure of the latest remote sensing technologies which provide regular and freely observations at continental scale, it has been already recognised the importance of harmonised landslide hazard and risk map at continental scale following the European landslide susceptibility map (Wilde et al., 2018). Such products will represent valuable outcomes for focussing resources and implement medium to long term precautionary measures in prevention, emergency and post-crisis mitigation phases. In particular, satellite platform and downstreaming services are supplying geomorphological/kinematic data and information which has been acknowledged to be the main obstacle for producing reliable landslide hazard and risk maps from MLAs (Nsengiyumva and Valentino, 2020).

The use of the proposed ML-based landslide risk assessment method can be therefore particular beneficial if dealing with large datasets at continental scale to be regularly updated considering that slides, flows and complex movements (usually evolving as slow-moving landslides) represent more than half of the 849,543 landslide events in Europe (Herrera et al., 2018). With this respect, the Termini-Nerano valley represents a perfect case study given the amount of high-resolution data available from remote sensing and ground-based techniques that have been used for developing, performing and validating for the first time this innovative solution where InSAR and MLAs are combined to produce a LRM.

Recent initiatives at continental scale work in favour of the replicability of our approach:

- InSAR datasets will be freely accessible at continental scale through the upcoming European Ground Motion Service (Crosetto et al., 2020) based on Sentinel-1 satellite data. This service will be of pivotal importance for landslide mapping activities at a national and regional scale.
- The MLAs used here are available for free across the most common statistics library of R-Studio and Python for example. MLAs are able to account for and large training datasets and EM, in particular, is a powerful tool which can account for different data-driven approaches together to regularly update or upscale landslide hazard maps.
- Data on population and buildings, from which V and E can be calculated, are nowadays easily accessible, homogenised and regularly collected at European level through the national statistics offices and made available at any user.

Further research, however, is needed to further develop the presented ML-based methodology in order to minimize subjectivity for selecting the different sources, resolution and mapping units associated with the input datasets, usually determined by the available datasets, and to extend it to different typologies of landslides.

## Declaration of Competing Interest

The authors declare that they have no known competing financial interests or personal relationships that could have appeared to influence the work reported in this paper.

## Acknowledgments

Many thanks are due to Italian Ministry of Environment and Protection of Land and Sea who supported the realization of the PST-A and to the European Space Agency, for the acquisition of the ENVISAT and COSMO-SkyMed imagery. This research was partially funded by the University of Naples Federico II and the Italian Compagnia di San Paolo Foundation (grant F.A.R.O. 2011) granted to Dipartimento di Scienze della Terra, dell'Ambiente e delle Risorse. A. Novellino performed the analysis during his PhD at the University of Naples and published with the permission of the Executive Director of the British Geological Survey (BGS-NERC). C.U.G.RI (Consortium between the Federico II University of Naples and the University of Salerno for the Prediction and Prevention of Major Hazards) is gratefully acknowledged for supporting this research with hardware/software facilities. The authors would like to acknowledge D. Boon and R. Ciurean from the British Geological Survey for their valuable suggestions to improve the quality of the paper.

## Appendix A. Supplementary material

Supplementary data to this article can be found online at https://doi.org/10.1016/j.catena.2021.105317.

## References

Alvarez, W., 1991. Tectonic evolution of the Corsica-Apennines-Alps region studied by the method of successive approximations. Tectonics 10 (5), 936–947. https://doi.org/10.1029/91TC00232.

Andrejev, K., Krušić, J., Đurić, U., Marjanović, M., Abolmasov, B., 2017. Relative Landslide Risk Assessment for the City of Valjevo. In: Workshop on World Landslide Forum. Springer, Cham, pp. 525–533.

Arabameri, A., Pradhan, B., Lombardo, L., 2019. Comparative assessment using boosted regression trees, binary logistic regression, frequency ratio and numerical risk factor for gully erosion susceptibility modelling. CATENA 183, 104223. https://doi.org/10.1016/j.catena.2019.104223.

Araujo, M.B., Pearson, R.G., Thuiller, W., Erhard, M., 2005. Validation of species-climate impact models under climate change. Glob. Change Biol. 11 (9), 1504–1513. https://doi.org/10.1111/j.1365-2486.2005.01000.x.

Aslan, G., Foumelis, M., Raucoules, D., De Michele, M., Bernardie, S., Cakir, Z., 2020. Landslide Mapping and Monitoring Using Persistent Scatterer Interferometry (PSI) Technique in the French Alps. Remote Sens. 12 (8), 1305. https://doi.org/10.3390/rs12081305.

Bartolini, S., Cappello, A., Martí, J., Del Negro, C., 2013. QVAST: a new Quantum GIS plugin for estimating volcanic susceptibility. Nat. Hazards Earth Syst. Sci. 13 (11), 3031–3042. https://doi.org/10.5194/nhess-13-3031-2013.

Bonì, R., Bosino, A., Meisina, C., Novellino, A., Bateson, L., McCormack, H., 2018. A methodology to detect and characterize uplift phenomena in urban areas using Sentinel-1 data. Remote Sens. 10 (4), 607. https://doi.org/10.3390/rs10040607.

Brugner, W., Valdinucci, A., 1973. Landslide classification scheme and correpsonding examples. Bollettino del Servizio Geologico d'Italia 73–110 (in Italian).

Canuti, P., Dramis, F., Esu, F., 1992. Stability conditions over urbanised slope: principles and general guidelines for public institutions. CNR-GNDCI, 544, 100 pp (in Italian).

Carlà, T., Raspini, F., Intrieri, E., Casagli, N., 2016. A simple method to help determine landslide susceptibility from spaceborne InSAR data: the Montescaglioso case study. Environ. Earth Sci. 75 (24), 1–12. https://doi.org/10.1007/s12665-016-6308-8.

Carotenuto, F., Angrisani, A.C., Bakthiari, A., Carratù, M.T., Di Martire, D., Finicelli, G.F., et al., 2017. A new statistical approach for landslide susceptibility assessment in the urban area of Napoli (Italy). In: Workshop on World Landslide Forum. Springer, Cham, pp. 881–889.

Casagli, N., Cigna, F., Bianchini, S., Hölbling, D., Füreder, P., Righini, G., et al., 2016. Landslide mapping and monitoring by using radar and optical remote sensing: Examples from the EC-FP7 project SAFER. Remote Sens. Appl.: Soc. Environ. 4, 92–108. https://doi.org/10.1016/j.rsase.2016.07.001.

Cesarano, M., Bish, D.L., Cappelletti, P., Cavalcante, F., Belviso, C., Fiore, S., 2018. Quantitative mineralogy of clay-rich siliciclastic landslide terrain of the Sorrento Peninsula, Italy, using a combined XRPD and XRF approach. Clays Clay Min 66 (4), 353–369. https://doi.org/10.1346/CCMN.2018.064108.

Chang, K.J., Chan, Y.C., Chen, R.F., Hsieh, Y.C., 2018. Geomorphological evolution of landslides near an active normal fault in northern Taiwan, as revealed by lidar and unmanned aircraft system data. Nat. Hazards Earth Syst. Sci. 18, 709–727. https://doi.org/10.5194/nhess-18-709-2018.

Chen, W., Pourghasemi, H.R., Kornejady, A., Zhang, N., 2017. Landslide spatial modeling: Introducing new ensembles of ANN, MaxEnt, and SVM machine learning techniques. Geoderma 305, 314–327. https://doi.org/10.1016/j.geoderma.2017.06.020.

Ciampalini, A., Raspini, F., Lagomarsino, D., Catani, F., Casagli, N., 2016. Landslide susceptibility map refinement using PSInSAR data. Remote Sens. Environ. 184, 302–315. https://doi.org/10.1016/j.rse.2016.07.018.

Cigna, F., Sowter, A., 2017. The relationship between intermittent coherence and precision of ISBAS InSAR ground motion velocities: ERS-1/2 case studies in the UK. Remote Sens. Environ. 202, 177–198. https://doi.org/10.1016/j.rse.2017.05.016.

Confuorto, P., Di Martire, D., Centolanza, G., Iglesias, R., Mallorqui, J.J., Novellino, A., et al., 2017. Post-failure evolution analysis of a rainfall-triggered landslide by multi-temporal interferometry SAR approaches integrated with geotechnical analysis. Remote Sens. Environ. 188, 51–72. https://doi.org/10.1016/j.rse.2016.11.002.

Costantini, M., Falco, S., Malvarosa, F., Minati, F., Trillo, F., Vecchioli, F., 2014. Persistent scatterer pair interferometry: approach and application to COSMO-SkyMed SAR data. IEEE J. Sel. Top. Appl. Earth Obs. Remote Sens. 7 (7), 2869–2879. https://doi.org/10.1109/JSTARS.2014.2343915.

Costantini, M., Ferretti, A., Minati, F., Falco, S., Trillo, F., Colombo, D., et al., 2017. Analysis of surface deformations over the whole Italian territory by interferometric processing of ERS, Envisat and COSMO-SkyMed radar data. Remote Sens. Environ. 202, 250–275. https://doi.org/10.1016/j.rse.2017.07.017G.

Cotecchia, V., Melidoro, G., 1966. Geological observation of the Termini-Nerano landslide. Geol. Appl. Idrogol 1, 93–122 (in Italian).

Crosetto, M., Solari, L., Mróz, M., Balasis-Levinsen, J., Casagli, N., Frei, M., et al., 2020. The Evolution of Wide-Area DInSAR: From Regional and National Services to the European Ground Motion Service. Remote Sens. 12 (12), 2043. https://doi.org/10.3390/rs12122043.

Cruden, D.M., Varnes, D.J., 1996. Landslide types and processes. In: Turner, A.K., Schuster, R.L. (Eds.), Landslides investigation and mitigation. Transportation research board. US National Research Council. Special Report 247, Washington, DC, pp. 36–75 (Chapter 3).

D'Argenio, B., Ferreri, V., Amodio, S., 2011. Eustatic cycles and tectonics in the Cretaceous shallow Tethys, Central-Southern Apennines. Italian J. Geosci. 130 (1), 119–127.

D'Elia, B., Picarelli, L., Leroueil, S., Vaunat, J., 1998. Geotechnical characterisation of slope movements in structurally complex clay soils and stiff jointed clays. Rivista Italiana di Geotecnica 32 (3), 5–47 (in Italian).

Dalla Via, G., Crosetto, M., Crippa, B., 2012. Resolving vertical and east-west horizontal motion from differential interferometric synthetic aperture radar: The L'Aquila earthquake. J. Geophys. Res. Solid Earth 117 (B2). https://doi.org/10.1029/2011JB008689.

Del Soldato, M., Riquelme, A., Bianchini, S., Tomàs, R., Di Martire, D., de Vita, P., et al., 2018. Multisource data integration to investigate one century of evolution for the Agnone landslide (Molise, southern Italy). Landslides 15 (11), 2113–2128. https://doi.org/10.1007/s10346-018-1015-z.

De Riso, R., Di Nocera, S., Pescatore, T., 2004. Special project for the study of unstable towns of the Campania Region - SCAI project, 1, 258-263. Napoli, 2004 (in Italian).

Di Martire, D., Tessitore, S., Brancato, D., Ciminelli, M.G., Costabile, S., Costantini, M., et al., 2016. Landslide detection integrated system (LaDIS) based on in-situ and satellite SAR interferometry measurements. Catena 137, 406–421. https://doi.org/10.1016/j.catena.2015.10.002.

Di Martire, D., Paci, M., Confuorto, P., Costabile, S., Guastaferro, S., Verta, A., et al., 2017. A nation-wide system for landslide mapping and risk management in Italy: The second Not-ordinary Plan of Environmental Remote Sensing. Int. J. Appl. Earth Obs. Geoinf. 36, 143–157. https://doi.org/10.1016/j.jag.2017.07.018.

Di Napoli, M., Carotenuto, F., Cevasco, A., Confuorto, P., Di Martire, D., Firpo, M., et al., 2020. Machine learning ensemble modelling as a tool to improve landslide susceptibility mapping reliability. Landslides 1–18. https://doi.org/10.1007/s10346-020-01392-9.

Dou, J., Yamagishi, H., Pourghasemi, H.R., Yunus, A.P., Song, X., Xu, Y., Zhu, Z., 2015. An integrated artificial neural network model for the landslide susceptibility assessment of Osado Island, Japan. Nat. Hazards 78 (3), 1749–1776. https://doi.org/10.1007/s11069-015-1799-2.

Elith, J., Graham, C.H., Anderson, R.P., Dudík, M., Ferrier, S., Guisan, A., et al., 2006. Novel methods improve prediction of species' distributions from occurrence data. Ecography 29 (2), 129–151. https://doi.org/10.1111/j.2006.0906-7590.04596.x.

Esu, F., 1977. Behaviour of slopes in structurally complex formations. In: Proceedings of the "International Symposium on the geotechnics of Structurally Complex Formations", Capri, pp. 292–304.

Fell, R., Corominas, J., Bonnard, C., Cascini, L., Leroi, E., Savage, W.Z., 2008. Guidelines for landslide susceptibility, hazard and risk zoning for land-use planning. Eng. Geol. 102 (3–4), 99–111. https://doi.org/10.1016/j.enggeo.2008.03.022.

Ferretti, A., Fumagalli, A., Novali, F., Prati, C., Rocca, F., Rucci, A., 2011. A new algorithm for processing interferometric data-stacks: SqueeSAR. IEEE Trans. Geosci. Remote Sens. 49 (9), 3460–3470. https://doi.org/10.1109/TGRS.2011.2124465.

Froude, M.J., Petley, D.N., 2018. Global fatal landslide occurrence from 2004 to 2016, 2018. Nat. Hazards Earth Syst. Sci. 18, 2161–2181. https://doi.org/10.5194/nhess-18-2161-2018.

Gariano, S.L., Guzzetti, F., 2016. Landslides in a changing climate. Earth Sci. Rev. 162, 227–252. https://doi.org/10.1016/j.earscirev.2016.08.011.

Handwerger, A.L., Huang, M., Fielding, E.J., Booth, A.M., Bürgmann, R., 2019. A shift from drought to extreme rainfall drives a stable landslide to catastrophic failure. Sci. Rep. 9, 1569. https://doi.org/10.1038/s41598-018-38300-0.

Herrera, G., Mateos, R.M., García-Davalillo, J.C., Grandjean, G., Poyiadji, E., Maftei, R., et al., 2018. Landslide databases in the Geological Surveys of Europe. Landslides 15 (2), 359–379. https://doi.org/10.1007/s10346-017-0902-z.

Hu, X., Bürgmann, R., Schulz, W.H., Fielding, E.J., 2020. Four-dimensional surface motions of the Slumgullion landslide and quantification of hydrometeorological forcing. Nat. Commun. 11, 2792. https://doi.org/10.1038/s41467-020-16617-7.

Huang, F., Cao, Z., Guo, J., Jiang, S.H., Li, S., Guo, Z., 2020. Comparisons of heuristic, general statistical and machine learning models for landslide susceptibility prediction and mapping. CATENA 191, 104580. https://doi.org/10.1016/j.catena.2020.104580.

Hungr, O., Leroueil, S., Picarelli, L., 2014. The Varnes classification of landslide types, an update. Landslides 11 (2), 167–194. https://doi.org/10.1007/s10346-013-0436-y.

Iannace, A., Capuano, M., Galluccio, L., 2011. "Dolomites and dolomites" in Mesozoic platform carbonates of the Southern Apennines: geometric distribution, petrography and geochemistry. Palaeogeogr. Palaeoclimatol. Palaeoecol. 310, 324–339. https://doi.org/10.1016/j.palaeo.2011.07.025.

ISPRA, 2015. Sheet index for Italian 1:50,000 geological series, sheet 466 "Sorrento". http://www.isprambiente.gov.it/Media/carg/note_illustrative/466_485_Sorrento_Termini.pdf (in Italian).

ISPRA, 2018. Hydrogeological instability in Italy: hazard and risk indicators. Report 2018 (in Italian).

ISTAT, 2011. Population Housing Census. Available at http://dati-censimentopopolazione.istat.it/Index.aspx?lang=en (accessed on 26/5/2020).

Jacobs, L., Kervyn, M., Reichenbach, P., Rossi, M., Marchesini, I., Alvioli, M., et al., 2020. Regional susceptibility assessments with heterogeneous landslide information: Slope unit-vs. pixel-based approach. Geomorphology 356, 107084. https://doi.org/10.1016/j.geomorph.2020.107084.

Kim, H.G., Lee, D.K., Park, C., Ahn, Y., Kil, S.-H., Sung, S., et al., 2018. Estimating landslide susceptibility areas considering the uncertainty inherent in modeling methods. Stoch. Env. Res. Risk A 32, 2987–3019. https://doi.org/10.1007/s00477-018-1609-y.

Lacroix, P., Handwerger, A.L., Bièvre, G., 2020. Life and death of slow-moving landslides. Nat. Rev. Earth Environ. 1, 404–419. https://doi.org/10.1038/s43017-020-0072-8.

Micheletti, N., Foresti, L., Robert, S., Leuenberger, M., Pedrazzini, A., Jaboyedoff, M., Kanevski, M., 2014. Machine learning feature selection methods for landslide susceptibility mapping. Math. Geosci. 46 (1), 33–57. https://doi.org/10.1007/s11004-013-9511-0.

Mililllo, P., Fielding, E.J., Shulz, W.H., Delbridge, B., Burgmann, R., 2014. COSMO-SkyMed spotlight interferometry over rural areas: The Slumgullion landslide in Colorado, USA. IEEE J. Sel. Top. Appl. Earth Obs. Remote Sens. 7 (7), 2919–2926. https://doi.org/10.1109/JSTARS.2014.2345664.

Mutti, E., Bernoulli, D., Ricci Lucchi, F., Tinterri, R., 2009. Turbidites and turbidity currents from Alpine 'flysch' to the exploration of continental margins. Sedimentology 56, 267–318. https://doi.org/10.1111/j.1365-3091.2008.01019.x.

Novellino, A., Cigna, F., Sowter, A., Syafiudin, M.F., Di Martire, D., Ramondini, M., et al., 2015. Intermittent small baseline subset (ISBAS) InSAR analysis to monitor landslides in Costa della Gaveta, Southern Italy. In: IEEE International Geoscience and Remote Sensing Symposium, IGARSS 2015; Milan; Italy. https://doi.org/10.1109/IGARSS.2015.7326584.

Novellino, A., Cigna, F., Sowter, A., Ramondini, M., Calcaterra, D., 2017. Exploitation of the Intermittent SBAS (ISBAS) algorithm with COSMO-SkyMed data for landslide inventory mapping in north-western Sicily, Italy. Geomorphology 280, 153–166. https://doi.org/10.1016/j.geomorph.2016.12.009.

Nsengiyumva, J.B., Valentino, R., 2020. Predicting landslide susceptibility and risks using GIS-based machine learning simulations, case of upper Nyabarongo catchment. Geomatics, Nat. Hazards Risk 11 (1), 1250–1277. https://doi.org/10.1080/19475705.2020.1785555.

Pappalardo, G., Mineo, S., Angrisani, A.C., Di Martire, D., Calcaterra, D., 2018. Combining field data with infrared thermography and DInSAR surveys to evaluate the activity of landslides: the case study of Randazzo Landslide (NE Sicily). Landslides 15 (11), 2173–2193. https://doi.org/10.1007/s10346-018-1026-9.

SAHD, 2011a. Landslide Inventory Map. Available at archive for the SAHD maps (accessed on 24/10/2018) (in Italian).

SAHD, 2011b. Landslide Risk Map. Available at archive for the SAHD maps (accessed on 10/5/2020) (in Italian).

SAHD, 2011c. Geomorphological Map. Available at archive for the SAHD maps (accessed on 12/5/2020) (in Italian).

Salvati, P., Bianchi, C., Rossi, M., Guzzetti, F., 2010. Societal landslide and flood risk in Italy. Nat. Hazards Earth Syst. Sci. 10, 465–483. https://doi.org/10.5194/nhess-10-465-2010.

Sepe, C., Confuorto, P., Angrisani, A.C., Di Martire, D., Di Napoli, M., Calcaterra, D., 2019. Application of statistical approach to landslide susceptibility map generation in urban settings. In: Proc IAEG/AEG Annu Meeting Proc., vol. 1. Springer, Cham, San Francisco, pp. 155–162.

Solari, L., Del Soldato, M., Raspini, F., Barra, A., Bianchini, S., Confuorto, P., Casagli, N., Crosetto, M., 2020. Review of satellite interferometry for landslide detection in Italy. Remote Sens. 12 (8), 1351. https://doi.org/10.3390/rs12081351.

Thai Pham, B., Shirzadi, A., Shahabi, H., Omidvar, E., Singh, S.K., Sahana, M., et al., 2019. Landslide susceptibility assessment by novel hybrid machine learning algorithms. Sustainability 11 (16), 4386. https://doi.org/10.3390/su11164386.

Thuiller, W., Lafourcade, B., Engler, R., Araújo, M.B., 2009. BIOMOD - a platform for ensemble forecasting of species distributions. Ecography 32, 369–373. https://doi.org/10.1111/j.1600-0587.2008.05742.x.

Van Westen, C.J., Castellanos, E., Kuriakose, S.L., 2008. Spatial data for landslide susceptibility, hazard, and vulnerability assessment: an overview. Eng. Geol. 102 (3–4), 112–131. https://doi.org/10.1016/j.enggeo.2008.03.010.

Vinci, F., Iannace, A., Parente, M., Pirmez, C., Torrieri, S., Giorgioni, M., 2017. Early dolomitization in the Lower Cretaceous shallow-water carbonates of Southern Apennines (Italy): Clues about palaeoclimatic fluctuations in western Tethys. Sed. Geol. 362, 17–36. https://doi.org/10.1016/j.sedgeo.2017.10.007.

Vitale, S., Tramparulo, F.D.A., Ciarcia, S., Amore, F.O., Prinzi, E.P., Laiena, F., 2017. The northward tectonic transport in the southern Apennines: examples from the Capri Island and western Sorrento Peninsula (Italy). Int. J. Earth Sci. 106 (1), 97–113. https://doi.org/10.1007/s00531-016-1300-9.

Wilde, M., Günther, A., Reichenbach, P., Malet, J.P., Hervás, J., 2018. Pan-European landslide susceptibility mapping: ELSUS Version 2. J. Maps 14 (2), 97–104. https://doi.org/10.1080/17445647.2018.1432511.